integrity Research Journals

Applied Journal of Physical Science
Volume 6(5), pages 184-198, December 2025
Article Number: 8AEA03033
ISSN: 2756-6684
https://doi.org/10.31248/AJPS2025.132
https://integrityresjournals.org/journal/AJPS

Full Length Research

Induced magnetic field effect on steady magnetohydrodynamic natural convection Couette flow with variable fluid properties in a vertical channel

Kabir M. Tafida*, Aisha Y. Abdullahi and Muhammed Yahuza

Department of Mathematics, Federal University of Education, Zaria, Nigeria.

*Corresponding author. Email: mktafida.555@gmail.com

Received 3rd October 2025; Accepted 18th November 2025

ABSTRACT: This study investigates steady magnetohydrodynamic (MHD) natural convection Couette flow in a vertical channel, incorporating temperature-dependent fluid properties, namely viscosity and thermal conductivity, to more accurately represent realistic flow behaviour. The analysis accounts for the induced magnetic field by the motion of the conducting fluid, and the governing momentum, energy, and magnetic induction equations are solved using the Homotopy Perturbation Method. Results show that decreasing viscosity with increasing temperature enhances fluid motion, whereas higher thermal conductivity improves heat distribution but may reduce flow acceleration. An increase in the Hartmann number suppresses fluid velocity due to stronger magnetic damping, while higher magnetic Prandtl numbers amplify the induced magnetic field. Additionally, reduced viscosity increases skin friction on the moving plate while decreasing it on the stationary plate. These findings offer valuable insights for a wide range of engineering and industrial applications, including cooling of electronic devices and nuclear reactors, MHD power generation, metallurgical process control, and thermal management in aerospace systems. They are also relevant to biomedical devices utilizing magnetic field-assisted fluid control, geothermal energy extraction, and advanced chemical reactors, where efficient heat and mass transfer under magnetic fields can improve overall performance and product quality.

Keywords: Homotopy perturbation method, induced magnetic field, natural convection, variable viscosity, variable thermal conductivity.

INTRODUCTION

Steady magnetohydrodynamic (MHD) natural convection Couette flow has garnered significant attention due to its importance in a wide range of industrial and engineering applications, including electronic device cooling, nuclear reactor safety, MHD power generation, and metallurgical processes such as crystal growth and liquid metal casting. It also plays a crucial role in aerospace engineering for the thermal management of high-temperature components and in biomedical engineering for controlling blood flow under magnetic field-assisted therapies. This study incorporates temperature-dependent fluid properties, such as viscosity and thermal conductivity, to more accurately capture real-world behaviour. Furthermore, the effect of the induced magnetic field resulting from the fluid's motion is considered, providing a more comprehensive representation of the flow dynamics. The main objective is to examine the combined impact of variable fluid properties and induced magnetic fields on the velocity and temperature distributions within a vertical channel under steady-state conditions, yielding insights valuable for the design and optimisation of industrial cooling systems, energy-efficient MHD devices, and safety protocols in nuclear and metallurgical operations.

Hamza *et al.* (2024a) observed that both temperature and velocity increase with enhanced variable thermal conductivity. Tafida and Ajibade (2019) concluded that skin friction on both plates increases as viscosity rises. Das and Patgiri (2024a) reported that higher viscosity and thermal conductivity parameters lead to a reduction in fluid velocity. In a separate study, Das and Patgiri (2024b)

found that an increase in the thermal conductivity parameter elevates the temperature. Ajibade and Ojeagbase (2019) highlighted that skin friction increases with higher thermal conductivity of the working fluid. Mottupalle *et al.* (2022) noted that a rise in the viscosity parameter reduces fluid velocity, it simultaneously increases fluid temperature. Saini *et al.* (2023) reported that both velocity and temperature are enhanced by increasing the viscosity variation parameter; however, higher Hartmann numbers tend to suppress them. Omokhuale and Ojemeri (2024) employed the Homotopy Perturbation Method to derive the governing equations. Tafida *et al.* (2021) demonstrated that increasing the fluid's thermal conductivity thickens the thermal boundary layer, thereby raising the temperature within the channel. Hamza *et al.* (2024b) concluded that the heat transfer rate on the plates and skin friction rise with increasing variable thermal conductivity. Tafida *et al.* (2020) found that increasing fluid viscosity leads to an elevated temperature profile. Bichi and Ajibade (2020) revealed that a reduction in viscosity results in increased fluid velocity. Saravanakumar (2023) concluded that fluid temperature increases with higher powers of the thermal conductivity function. Kaita *et al.* (2024) showed that a rise in the thermal conductivity parameter decreases the rate of heat transfer on the moving plate. Sharahy and Sawlan (2023) reported that their numerical method effectively estimated temperature-dependent thermal properties. Borgohain (2023) emphasised that the viscosity parameter favours temperature elevation, while increased thermal conductivity reduces the thickness of the thermal boundary layer. Ajibade and Umar (2020) observed a decline in velocity near the heated plate with increased viscosity and thermal conductivity. Ajibade and Tafida (2020) concluded that fluid velocity decreases with increasing viscosity, and both velocity and temperature decrease as thermal conductivity increases. Jha and Aina (2017) reported that accounting for the induced magnetic field results in higher velocity profiles compared to when it is neglected. Tafida and Tajuddeen (2024) applied the Homotopy perturbation method to solve coupled nonlinear differential equations. Sobamowo (2023) noted that the Homotopy perturbation method is effective for determining complex roots of nonlinear equations. Farhood and Mohammed (2023) emphasised the method's efficiency and its capability to ensure rapid solution convergence due to its simplicity. Abdul-Ameer and Abdul-Sattar (2023) reported that the Homotopy perturbation method (HPM) is both reliable and accurate. Erinle-Ibrahim *et al.* (2021) highlighted its effectiveness as an approximation technique for solving temperature equations. Likewise, Gouder *et al.* (2022) concluded that the Homotopy perturbation method not only delivers accurate solutions but also ensures faster convergence with minimal computational effort. Ajibade and Bolaji (2020) reported that increasing the fluid viscosity, magnetic Prandtl number and Hartmann number, as well as reducing the conductivity of the working fluid, hinders the velocity distribution of the flow. Jha and Malgwi (2022) observed that a higher Hartmann number decreases the velocity distribution along the vertical main flow direction for both symmetric and asymmetric wall heating, while enhancing it along the induced flow direction. Sobamowo (2023) established the capability of the Homotopy perturbation method (HPM) in determining complex roots of nonlinear equations. Similarly, Khaleghizadeh (2022) emphasised the power and efficiency of the Homotopy perturbation method in solving nonlinear problems. Adnan and Osama (2023) further highlighted the method's remarkable simplicity, effectiveness and rapid convergence. Tafida *et al.* (2025) successfully applied the Homotopy perturbation method to solve the governing momentum and energy equations. Reddy *et al.* (2022) concluded that the heat transfer gradient increases with the Prandtl number, while a reduction is observed in the presence of variable fluid properties.

Kandagal and Kempepatil (2024) reported that viscosity has a significant influence on heat and momentum transfer in porous media. Kumar *et al.* (2023) concluded that increasing the thermal conductivity and viscosity ratio enhances the flow in both regions. Kalyan *et al*. (2025) found that viscosity variations lead to a reduction in velocity. Kandagal *et al.* (2025) reported that the addition of CNTs significantly enhances the thermal conductivity of both engine oil and blood suspensions, resulting in improved heat dissipation. Konduru *et al.* (2024) highlighted that their results provide an important understanding of system behaviour under diverse physical conditions, thereby enhancing the overall knowledge of heat and mass transfer in complex fluids. Jyothi *et al.* (2025) concluded that the findings of this study may have significant applications in geothermal energy systems, microelectronics, and other domains involving MHD-driven heat and mass transfer processes. Meruva *et al.* (2022) reported that their study focuses on the heat and mass transfer characteristics of three-dimensional magnetohydrodynamic flow. Umamaheswar *et al.* (2022) concluded that an increase in the Prandtl number results in a significant rise in skin friction.

To examine the combined influence of temperature-dependent fluid properties and induced magnetic fields on MHD Couette flow, providing a quantitative understanding of their interactions. The results are directly relevant to engineering applications, including electronic device cooling, MHD power generation, metallurgical processes, and thermal management in aerospace systems.

PROBLEM FORMULATION

A steady magnetohydrodynamic (MHD) flow of a viscous, incompressible, and electrically conducting fluid with constant density, confined between two vertical parallel plates separated by a distance h was considered (Figure 1). A constant heat flux is applied to the plate at $y^* = 0$, while the opposite plate at $y^* = h$ is maintained at a fixed

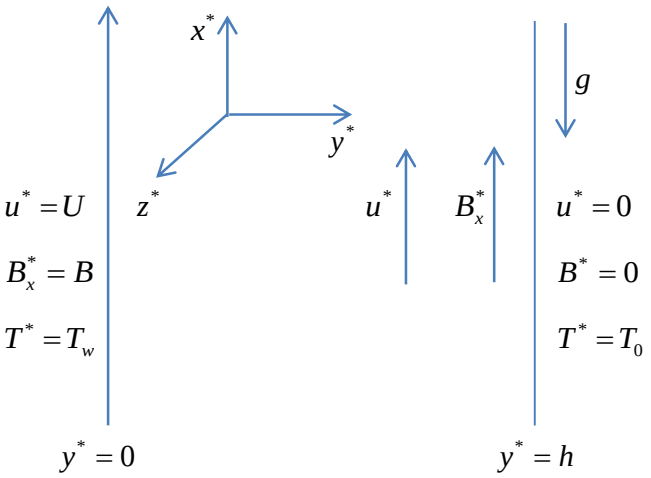

Figure 1. Diagrammatic representation of the flow.

temperature. Here, u^* and v^* denote the velocity components along the x^* and y^*-directions, respectively. However, due to the flow geometry, the fluid velocity is assumed to vary only along the transverse coordinate y^*. A uniform transverse magnetic field of strength B_0^* is imposed in the direction of the flow x^*. The plate at $y^* = 0$ is electrically non-conducting, whereas the plate at $y^* = h$ is conducting. The electrical conductivity of the fluid (σ) leads to the induction of a magnetic field $B_{x^*}^*$ along the $x-$axis. Furthermore, ρ represents the fluid density and c_p denotes the specific heat at constant pressure.

The dimensional momentum and energy governing equations, formulated within the framework of the Boussinesq approximation, are given as follows:

$$\frac{1}{\rho}\frac{d}{dy^*}\left(\mu^*\frac{du^*}{dy^*}\right)+\frac{\mu_e B_0}{\rho}\frac{dB_{x^*}^*}{dy^*}+g\beta\left(T^*-T_0^*\right)=0, \quad (1)$$

$$\frac{1}{\sigma\mu_e}\frac{d^2B_{x^*}^*}{dy^{*2}}+B_0^*\frac{du^*}{dy^*}=0, \quad (2)$$

$$\frac{1}{\rho cp}\frac{d}{dy^{\wedge}}\left(k^*\frac{dT^*}{dy^*}\right)=0 \quad (3)$$

Equation (1) represents the momentum equation, where the first term incorporates the effect of variable viscosity. The viscosity is modelled as an inverse function of temperature, as proposed by Singh and Argawal (2013). That is

$$\frac{1}{\mu^*}=\frac{1}{\mu_0}(1+a(T^*-T_0)) \quad (4)$$

Equation (2) represents the expression for the induced magnetic field, while equation (3) denotes the energy equation, incorporating variable thermal conductivity as proposed by Hazarika and Konch 2016), is expressed as follows:

$$\frac{1}{k^*}=\frac{1}{k_0}(1+b(T^*-T_0)) \quad (5)$$

Here, a, b and T_0 are constants determined by the standard state and thermal properties, that is υ represents the kinematic viscosity, and k^* denotes the thermal conductivity of the fluid. For liquids, the value of $(a>0)$, whereas for gases, $(a<0)$. Additionally, μ_0 and k_0 refer to the dynamic viscosity and thermal conductivity of the fluid far from the wall, respectively.

The boundary conditions are given as:

$$u^* = U,\ B^*_{x^*} = B,\ T^* = T_w \text{ at } y^* = 0,$$
$$u^* = 0,\ B^*_{x^*} = 0,\ T^* = T_0 \text{ at } y^* = h. \quad (6)$$

Here, U denotes the velocity of the moving plate, T_w represents the temperature of the heated plate, and T_0 indicates the temperature of the cold plate. The dimensionless parameters employed in equations (1), (2), and (3), along with the boundary conditions specified in equation (6), are defined as follows.

$$y = \frac{y^*}{h}, u = \frac{\nu_0 u^*}{g\beta h^2 \Delta T^*}, B = \frac{\nu^*}{g\beta h^2 \Delta T^*}\sqrt{\frac{\mu_e}{\rho}}B^*_{x^*}\lambda = a\Delta T, \varepsilon = b\Delta T,$$
$$Pm = \nu_0\sigma\mu_e, \Delta T^* = \frac{hq}{k}, T = \frac{T^* - T_0^*}{\Delta T^*}, Ha = \frac{B_0 h}{\nu_0}\sqrt{\frac{\mu_e}{\rho}}. \quad (7)$$

Here, y represents the non-dimensional temperature, u denotes the non-dimensional velocity and B corresponds to the non-dimensional induced magnetic field. Pm is the non-dimensional magnetic Prandtl number, λ refers to the non-dimensional viscosity parameter and ε denotes the non-dimensional thermal conductivity parameter. Additionally, T is the non-dimensional fluid temperature, Ha represents the non-dimensional Hartmann number, B_0 is the constant magnetic flux, μ_e denotes the magnetic permeability, β is the coefficient of thermal expansion, ρ represents the fluid density, and σ denotes the electrical conductivity of the fluid, respectively.
The governing momentum, energy and induced magnetic field equations (1), (2), and (3) are expressed in non-dimensional form as a set of nonlinear second-order ordinary differential equations (8), (9) and (10). Together with the boundary conditions given in equation (6), they are transformed as follows:

$$\frac{d^2u}{dy^2} - \lambda(1+\lambda T)\frac{du}{dy}\frac{dT}{dy} + Ha\frac{dB}{dy} + (1+\lambda T)T = 0, \quad (8)$$

$$\frac{d^2B}{dy^2} + PmHa\frac{du}{dy} = 0, \quad (9)$$

$$\frac{d^2T}{dy^2} - \varepsilon(1+\varepsilon T)\left(\frac{dT}{dy}\right)^2 = 0, \quad (10)$$

Here, λ denotes the viscosity parameter, Ha is the Hartmann number, Pm represents the magnetic Prandtl number and ε is the thermal conductivity parameter.

The corresponding boundary conditions are reformulated and incorporated into equation (11) as follows:

$$u = 1,\ B = 1,\ T = 1 \text{ at } y = 0,$$
$$u = 0,\ B = 0,\ T = 0 \text{ at } y = 1. \quad (11)$$

METHOD OF SOLUTION

Equations (8) – (10) are solved using Homotopy Perturbation Method (HPM). By constructing a convex homotopy, the momentum, energy and induced magnetic field equations, along with the boundary conditions are addressed as outlined below:

$$H(u,p)=(1-p)\left(\frac{d^2u}{dy^2}\right)+p\left(\frac{d^2u}{dy^2}-\lambda(1+\lambda T)\frac{du}{dy}\frac{dT}{dy}+Ha\frac{dB}{dy}+(1+\lambda T)T\right)=0, \quad (12)$$

$$H(B,p)=(1-p)\left(\frac{d^2B}{dy^2}\right)+p\left(\frac{d^2B}{dy^2}+PmHa\frac{du}{dy}\right)=0. \quad (13)$$

$$H(T,p)=(1-p)\left(\frac{d^2T}{dy^2}\right)+p\left(\frac{d^2T}{dy^2}-\varepsilon(1+\varepsilon T)\left(\frac{dT}{dy}\right)^2\right)=0. \quad (14)$$

Thus, in the absence of an initial approximation, the equation takes the following form:

$$\frac{d^2u}{dy^2}=p\left(\lambda(1+\lambda T)\frac{du}{dy}\frac{dT}{dy}-Ha\frac{dB}{dy}-(1+\lambda T)T\right) \quad (15)$$

$$\frac{d^2B}{dy^2}=p\left(-PmHa\frac{du}{dy}\right) \quad (16)$$

$$\frac{d^2T}{dy^2}=p\left(\varepsilon(1+\varepsilon T)\left(\frac{dT}{dy}\right)^2\right) \quad (17)$$

The solutions of equations (8), (9) and (10) are written in the following form:

$$u=u_0+pu_1+p^2u_2+p^3u_3+..., \quad (18)$$

$$B=B_0+pB_1+p^2B_2+p^3B_3+..., \quad (19)$$

$$T=T_0+pT_1+p^2T_2+p^3T_3+..., \quad (20)$$

Substituting equation (18) into equation (15), equation (19) into equation (16) and equation (20) into equation (17) yields the following results:

$$\begin{aligned}\frac{d^2u_0}{dy^2}+p\frac{d^2u_1}{dy^2}+p^2\frac{d^2u_2}{dy^2}+...=p\left(\lambda\left(\frac{du_0}{dy}\frac{dT_0}{dy}+\lambda T_0\frac{du_0}{dy}\frac{dT_0}{dy}\right)-Ha\frac{dB_0}{dy}-T_0-\lambda T_0^2\right)\\ +p^2\left(\lambda\left(\frac{du_1}{dy}\frac{dT_0}{dy}+\frac{du_0}{dy}\frac{dT_1}{dy}\right)+\lambda^2T_0\left(\frac{du_1}{dy}\frac{dT_0}{dy}+\frac{du_0}{dy}\frac{dT_1}{dy}\right)+\lambda^2T_1\frac{du_0}{dy}\frac{dT_0}{dy}\right)\\ +p^2\left(-Ha\frac{dB_1}{dy}-T_1-2\lambda T_0T_1\right)+...\end{aligned} \quad (21)$$

$$\frac{d^2B_0}{dy^2}+p\frac{d^2B_1}{dy^2}+p^2\frac{d^2B_2}{dy^2}+...=-p\left(PmHa\frac{du_0}{dy}\right)-p^2\left(PmHa\frac{du_1}{dy}\right)-... \quad (22)$$

$$\frac{d^2T_0}{dy^2} + p\frac{d^2T_1}{dy^2} + p^2\frac{d^2T_2}{dy^2} + \ldots = p\left(\varepsilon\left(\frac{dT_0}{dy}\right)^2 + \varepsilon^2 T_0\left(\frac{dT_0}{dy}\right)^2\right)$$

$$+ p^2\left(2\varepsilon\frac{dT_0}{dy}.\frac{dT_1}{dy} + 2\varepsilon^2 T_0\frac{dT_0}{dy}\frac{dT_1}{dy} + \varepsilon^2 T_1\left(\frac{dT_0}{dy}\right)^2 + \right)\ldots \quad (23)$$

Equating the coefficient of the corresponding terms of p^0, p^1, p^2 and p^3 in equations (21), (22), and (23) yields:

$$p^0 : \frac{d^2u_0}{dy^2} = 0, \quad (24)$$

$$p^0 : \frac{d^2B_0}{dy^2} = 0, \quad (25)$$

$$p^0 : \frac{d^2T_0}{dy^2} = 0, \quad (26)$$

$$p^1 : \frac{d^2u_1}{dy^2} = \lambda\frac{du_0}{dy}\frac{dT_0}{dy} + \lambda^2 T_0\frac{du_0}{dy}\frac{dT_0}{dy} - Ha\frac{dB_0}{dy} - T_0 - \lambda T_0^2, \quad (27)$$

$$p^1 : \frac{d^2B_1}{dy^2} = -PmHa\frac{du_0}{dy}, \quad (28)$$

$$p^1 : \frac{d^2T_1}{dy^2} = \varepsilon\left(\frac{dT_0}{dy}\right)^2 + \varepsilon^2 T_0\left(\frac{dT_0}{dy}\right)^2, \quad (29)$$

$$p^2 : \frac{d^2u_2}{dy^2} = \lambda\frac{du_1}{dy}\frac{dT_0}{dy} + \lambda\frac{du_0}{dy}\frac{dT_1}{dy} + \lambda^2 T_0\frac{du_1}{dy}\frac{dT_0}{dy} + \lambda^2 T_0\frac{du_0}{dy}\frac{dT_1}{dy}$$
$$+ \lambda^2 T_1\frac{du_0}{dy}\frac{dT_0}{dy} - Ha\frac{dB_1}{dy} - T_1 - 2\lambda T_0 T_1, \quad (30)$$

$$p^2 : \frac{d^2B_2}{dy^2} = -PmHa\frac{du_1}{dy}, \quad (31)$$

$$p^2 : \frac{d^2T_2}{dy^2} = 2\varepsilon\frac{dT_0}{dy}\frac{dT_1}{dy} + 2\varepsilon^2 T_0\frac{dT_0}{dy}\frac{dT_1}{dy} + \varepsilon^2 T_1\left(\frac{dT_0}{dy}\right)^2, \quad (32)$$

The boundary condition specified in equation (11) is rewritten as:

$$\left.\begin{array}{l} u_0(0) = 1, u_1(0) = u_2(0) = u_3(0) = \ldots = 0, \\ u_0(1) = u_1(1) = u_2(1) = u_3(1) = \ldots = 0, \\ B_0(0) = 1, B_1(0) = B_2(0) = B_3(0) = \ldots = 0, \\ B_0(1) = B_1(1) = B_2(1) = B_3(1) = \ldots = 0, \\ T_0(0) = 1, T_1(0) = T_2(0) = T_3(0) = \ldots = 0, \\ T_0(1) = T_1(1) = T_2(1) = T_3(1) = \ldots = 0. \end{array}\right\} \quad (33)$$

Equations (34), (35) and (36) are obtained by applying equations (24), (25) and (26) together with the boundary conditions $u_0(0)=1$ and $u_0(1)=0$, $B_0(0)=1$ and $B_0(1)=0$, $T_0(0)=1$ and $T_0(1)=0$ and performing the necessary computations, as shown below:

$$u_0 = A_1 y + A_2, \tag{34}$$

$$B_0 = B_1 y + B_2, \tag{35}$$

$$T_0 = C_1 y + C_2. \tag{36}$$

Equations (37), (38) and (39) are obtained by applying equations (27), (28) and (29) together with the boundary conditions $u_1(0)=0$ and $u_1(1)=0$, $B_1(0)=0$ and $B_1(1)=0$, $T_1(0)=0$ and $T_1(1)=0$ and performing the necessary computations, as shown below:

$$u_1 = \frac{\lambda y^2}{2} + \lambda^2\left(\frac{y^2}{2}-\frac{y^3}{6}\right) + \frac{Hay^2}{2} - \left(\frac{y^2}{2}-\frac{y^3}{6}\right) - \lambda\left(\frac{y^2}{2}-\frac{y^3}{3}+\frac{y^4}{12}\right) + A_3 y + A_4, \tag{37}$$

$$B_1 = \frac{PmHay^2}{2} + B_3 y + B_4. \tag{38}$$

$$T_1 = \frac{\varepsilon y^2}{2} + \varepsilon^2\left(\frac{y^2}{2}-\frac{y^3}{6}\right) + C_3 y + C_4. \tag{39}$$

Equations (40), (41) and (42) are obtained by applying equations (30), (31) and (32) together with the boundary conditions $u_2(0)=0$ and $u_2(1)=0$, $B_2(0)=0$ and $B_2(1)=0$, $T_2(0)=0$ and $T_2(1)=0$ and performing the necessary computations, as shown below:

$$\begin{aligned} u_2 = {} & -\frac{\lambda\varepsilon y^3}{6} - \lambda\varepsilon^2\left(\frac{y^3}{6}-\frac{y^4}{24}\right) - \frac{\lambda C_3 y^2}{2} - \frac{\lambda^3 y^3}{6} - \lambda^4\left(\frac{y^3}{6}-\frac{y^4}{24}\right) - \frac{\lambda^2 Hay^3}{6} + \lambda^2\left(\frac{y^3}{6}-\frac{y^4}{24}\right) \\ & + \lambda^3\left(\frac{y^3}{6}-\frac{y^4}{12}+\frac{y^5}{60}\right) - \frac{\lambda^2 A_3 y^2}{2} + \frac{\lambda^3 y^4}{12} + \lambda^4\left(\frac{y^4}{12}-\frac{y^5}{40}\right) - \frac{\lambda^2 Hay^4}{12} - \lambda^2\left(\frac{y^4}{12}-\frac{y^5}{40}\right) \\ & - \lambda^3\left(\frac{y^4}{12}-\frac{y^5}{20}+\frac{y^6}{90}\right) + \frac{\lambda^2 A_3 y^3}{6} - \frac{\lambda^2\varepsilon y^3}{6} - \lambda^2\varepsilon^2\left(\frac{y^3}{6}-\frac{y^4}{24}\right) - \frac{\lambda^2 C_3 y^2}{2} + \frac{\lambda^2\varepsilon y^4}{8} + \frac{\lambda^2 C_3 y^3}{3} \\ & + \lambda^2\varepsilon^2\left(\frac{y^4}{12}-\frac{y^5}{40}\right) + \frac{\lambda\varepsilon y^5}{20} + \lambda^2\varepsilon^2\left(\frac{y^4}{24}-\frac{y^5}{120}\right) - \frac{PmHa^2 y^3}{6} - \frac{HaB_3 y^2}{2} - \frac{\varepsilon y^3}{12} - \frac{C_3 y^3}{6} \\ & - \varepsilon^2\left(\frac{y^4}{24}-\frac{y^5}{120}\right) - \frac{\lambda\varepsilon y^4}{12} - \lambda\varepsilon^2\left(\frac{y^4}{12}-\frac{y^5}{60}\right) - \frac{2\lambda C_3 y^3}{3} + \lambda\varepsilon^2\left(\frac{y^5}{20}-\frac{y^6}{90}\right) + A_5 y + A_6 \end{aligned} \tag{40}$$

$$\begin{aligned} B_2 = {} & -\frac{\lambda PmHay^3}{6} - \lambda^2 PmHa\left(\frac{y^3}{6}-\frac{y^4}{24}\right) + PmHa\left(\frac{y^3}{6}-\frac{y^4}{24}\right) + \lambda PmHa\left(\frac{y^3}{6}-\frac{y^4}{12}+\frac{y^5}{60}\right) \\ & - \frac{PmHa^2 y^3}{6} - - \frac{PmHaA_3 y^2}{2} + B_5 y + B_6 \end{aligned} \tag{41}$$

$$T_2 = -\frac{\varepsilon^2 y^2}{3} - \varepsilon^3\left(\frac{y^3}{3} - \frac{y^4}{12}\right) - \varepsilon C_3 y^2 - \frac{\varepsilon^3 y^3}{3} - \varepsilon^4\left(\frac{y^3}{3} - \frac{y^4}{12}\right) - \varepsilon^2 C_3 y^2 + \frac{\varepsilon^3 y^4}{6}$$
$$+ \varepsilon^4\left(\frac{y^4}{6} - \frac{y^5}{20}\right) + \frac{\varepsilon^2 C_3 y^3}{3} + \frac{\varepsilon^3 y^4}{24} + \varepsilon^4\left(\frac{y^4}{24} - \frac{y^5}{120}\right) + \frac{\varepsilon^2 C_3 y^3}{6} + C_5 y + C_6, \quad (42)$$

Where:

$A_1 = B_1 = C_1 = -1,$

$A_2 = B_2 = C_2 = 1,$

$A_3 = \frac{1}{3} - \frac{\lambda}{4} - \frac{\lambda^2}{4} - \frac{Ha}{2}, \quad A_4 = 0,$

$B_3 = -\frac{PmHa}{2}, \quad B_4 = 0,$

$C_3 = -\frac{\varepsilon}{2} - \frac{\varepsilon^2}{3}, \quad C_4 = 0,$

$$A_5 = -\frac{\lambda}{8} + \frac{\lambda A_3}{2} + \frac{\lambda Ha}{6} + \frac{\lambda^3}{8} + \frac{\lambda\varepsilon}{5} + \frac{\lambda\varepsilon^2}{12} + \frac{\lambda C_3}{2} + \frac{\lambda^3}{36} + \frac{\lambda^4}{15} + \frac{\lambda^2 Ha}{12} + \frac{\lambda^2 A_3}{3} + \frac{\lambda^2\varepsilon}{24}$$
$$+ \frac{\lambda^2\varepsilon^2}{30} + \frac{\lambda^2 C_3}{6} + \frac{PmHa^2}{6} + \frac{HaB_3}{2} + \frac{\varepsilon}{24} + \frac{\varepsilon^2}{30} + \frac{C_3}{6}$$

$$B_5 = \frac{\lambda PmHa}{6} + \frac{\lambda^2 PmHa}{8} + \frac{PmHa^2}{8} - \frac{PmHa}{8} - \frac{\lambda PmHa}{10} + \frac{PmHaA_3}{2},$$

$$C_5 = \frac{\varepsilon^2}{3} + \frac{3\varepsilon^3}{8} + \varepsilon C_3 + \frac{\varepsilon^4}{10} + \frac{2\varepsilon^2 C_3}{3} - \frac{\varepsilon^2 C_3}{6}.$$

$A_6 = B_6 = C_6 = 0.$

Equations (34) – (42) present the approximate solutions for velocity, induced magnetic field and temperature as follows:

$$u = u_0 + u_1 + u_2 + ..., \quad (43)$$

$$B = B_0 + B_1 + B_2 + ..., \quad (44)$$

$$T = T_0 + T_1 + T_2 + ... \quad (45)$$

The skin friction at the channel boundaries is determined by taking the derivative of equation (43) with respect to y and evaluating it at $y = 0$ and $y = 1$ as given below:

$$\tau_0 = (1 - \lambda T)\left.\frac{du}{dy}\right|_{y=0} = (-1 + A_3 + A_5), \quad (46)$$

$$\tau_1 = (1-\lambda T)\frac{du}{dy}\bigg|_{y=1} = -\frac{3}{2}+\frac{2\lambda}{3}+\frac{5\lambda^2}{8}+Ha+A_3-\frac{7\lambda\varepsilon}{12}-\frac{2\lambda\varepsilon^2}{5}-\lambda C_3-\frac{\lambda^3}{15}-\frac{\lambda^4}{8}$$
$$-\frac{\lambda^2 Ha}{6}-\frac{\lambda^2 A_3}{2}-\frac{PmHa^2}{2}-HaB_3-\frac{\varepsilon}{6}-\frac{\varepsilon^2}{8}-\frac{C_3}{3}+A_5. \quad (47)$$

The heat transfer at the channel boundaries is determined by taking the derivative of equation (45) with respect to y and evaluating it at $y=0$ and $y=1$ as given below:

$$Nu_0 = (1-\varepsilon T)\frac{dT}{dy}\bigg|_{y=0} = -1+C_3+C_5, \quad (48)$$

$$Nu_1 = (1-\varepsilon T)\frac{dT}{dy}\bigg|_{y=1} = -1+\varepsilon-\frac{4\varepsilon^2}{3}+C_3--2\varepsilon C_3-\frac{\varepsilon^4}{8}-\frac{\varepsilon^2 C_3}{2}+C_5. \quad (49)$$

RESULTS AND DISCUSSION

This study considers temperature dependent fluid properties, including viscosity and thermal conductivity, to more accurately reflect realistic physical behaviour. Furthermore, the analysis incorporates the influence of the magnetic field generated by the motion of the conducting fluid, thereby offering a more detailed representation of the flow dynamics. The study aims to explore the combined effects of variable fluid properties and the induced magnetic field on the velocity and temperature distributions within a vertical channel under steady-state conditions. To achieve this, the governing momentum, energy and magnetic field equations (1), (2) and (3) are solved analytically using the Homotopy perturbation method in order to see the impacts of critical physical parameters.

Figure 2 shows the effect of temperature-dependent viscosity on the fluid's velocity distribution. As the variable viscosity parameter decreases, the fluid viscosity reduces with increasing temperature, which lowers viscous resistance and promotes greater fluid motion. This leads to a marked increase in the velocity profile across the channel. Conversely, when the viscosity parameter approaches zero, viscosity remains constant, resulting in higher resistance to flow and consequently lower velocity profiles. The figure clearly demonstrates that temperature-dependent viscosity enhances fluid mobility, particularly in regions subjected to elevated temperatures. These observations are highly relevant to several engineering and industrial applications. Temperature-dependent viscosity plays an important role in improving the efficiency of electronic cooling systems and optimising heat transfer in nuclear reactors. It also improves control over molten metal flow in metallurgical processes and enhances thermal management in high-temperature aerospace components. Furthermore, understanding viscosity variations is crucial for advancing polymer extrusion technologies and improving lubrication performance in automotive and mechanical systems.

Figure 3 illustrates how variations in the Hartmann number influence the velocity distribution of the conducting fluid. As the Hartmann number increases, the corresponding intensification of the Lorentz force produces a stronger opposing effect on the flow, resulting in reduced fluid velocity. This behaviour confirms that in magnetohydrodynamic (MHD) systems, higher Hartmann numbers, indicating stronger magnetic fields, introduce substantial magnetic damping and, consequently, a more significant suppression of fluid motion. The figure clearly demonstrates the dominant role of magnetic forces in governing the flow characteristics. This phenomenon holds considerable relevance in many practical settings. Effective regulation of liquid metal flow in MHD generators, for example, depends on controlling the Hartmann number. Similarly, the same principle aids in improving cooling performance in nuclear reactors and maintaining stable conditions during metallurgical processes such as continuous steel casting. It also contributes to better thermal management in electronic devices subjected to magnetic fields. In addition, understanding Hartmann-number-induced flow modulation is crucial for the design of fusion reactor coolant systems and for biomedical applications involving magnetic field-assisted blood flow control or targeted drug delivery.

Figures 4 and 5 present the velocity and temperature profiles, respectively, for various values of the thermal conductivity parameter. As shown in Figure 4, a decrease in thermal conductivity increases the fluid velocity, primarily because weaker heat diffusion produces steeper temperature gradients that promote stronger buoyancy-driven motion. In contrast, Figure 5 shows that higher

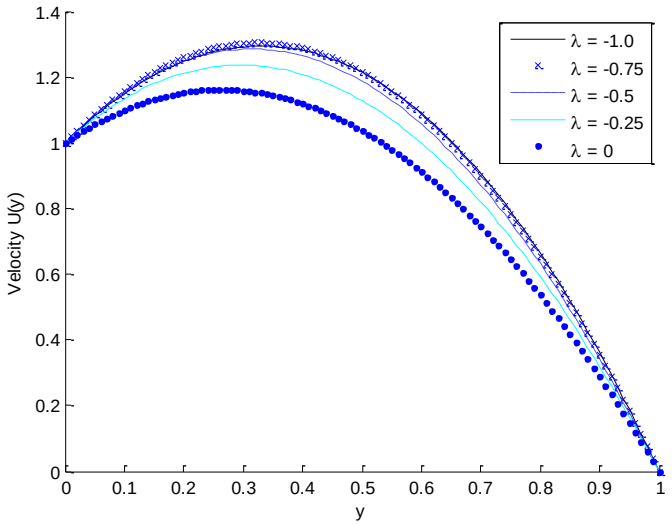

Figure 2. Effect of λ on velocity profile for different values of $(\varepsilon = 0.1, Ha = 4.0,\ \ Pm = 0.4)$.

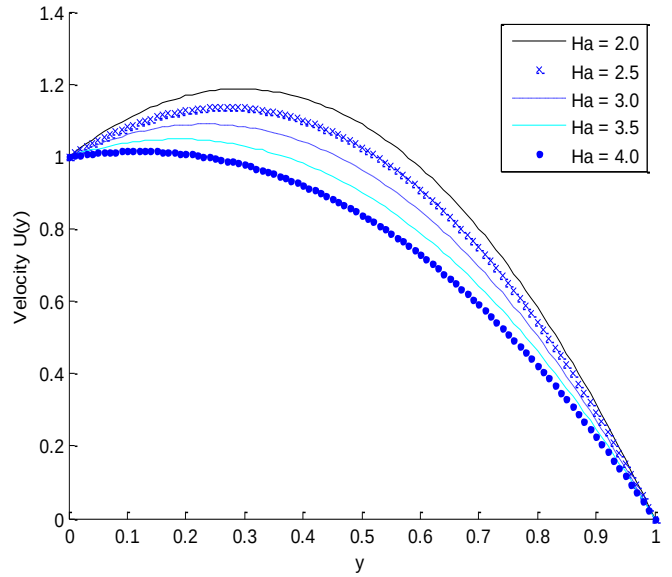

Figure 3. Effect of Ha on velocity profile for different values of $(\varepsilon = 0.1, Pm = 0.4,\ \lambda = -1.0)$

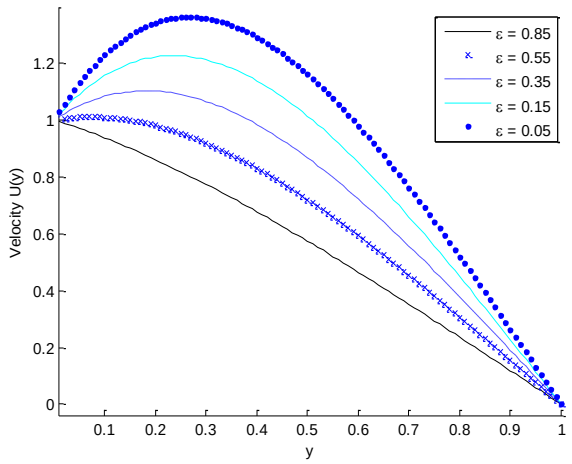

Figure 4. Effect of ε on velocity profile for different values of $(Ha = 4.0, Pm = 0.4,\ \lambda = -1.0)$

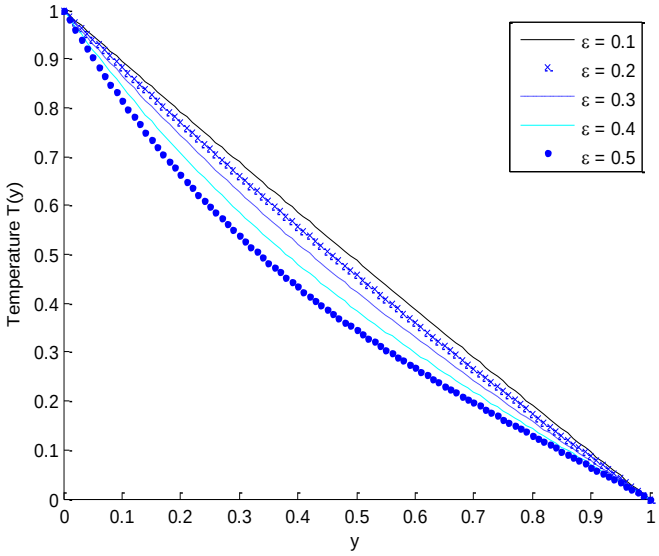

Figure 5. Effect of ε on temperature profile for different values of $(Ha = 4.0, Pm = 0.4,\ \lambda = -1.0)$.

thermal conductivity results in a more uniform temperature distribution, raising the overall fluid temperature while potentially reducing flow acceleration due to diminished thermal gradients. This behaviour underscores the competing effects of thermal conductivity on momentum and heat transport within the channel. These observations have several practical applications. Understanding the influence of thermal conductivity is crucial for designing efficient cooling systems for electronic devices and improving the performance of industrial heat exchangers. It also plays a significant role in thermal management within nuclear reactors and in regulating molten metal flow during metallurgical processes. Additionally, these insights support the development of advanced aerospace cooling systems for high-temperature components and enhance the efficiency of solar thermal collectors, where precise control of heat transfer and fluid motion is essential. Further applications include polymer processing, where temperature uniformity affects product quality, and geothermal energy extraction, where thermal conductivity strongly influences heat recovery rates.

As shown in Figure 6, a decrease in the magnetic Prandtl number corresponds to a reduced influence of the magnetic field on the fluid flow due to increased magnetic

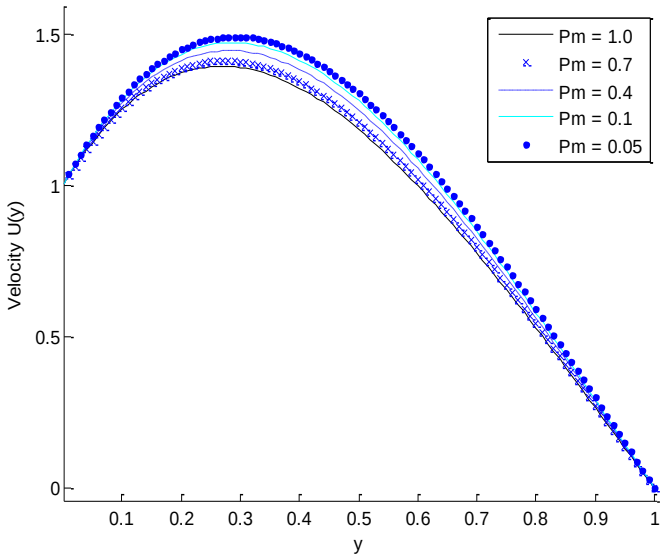

Figure 6. Effect of Pm on velocity profile for different values of $(Ha = 4.0, \varepsilon = 0.1,\ \lambda = -1.0)$

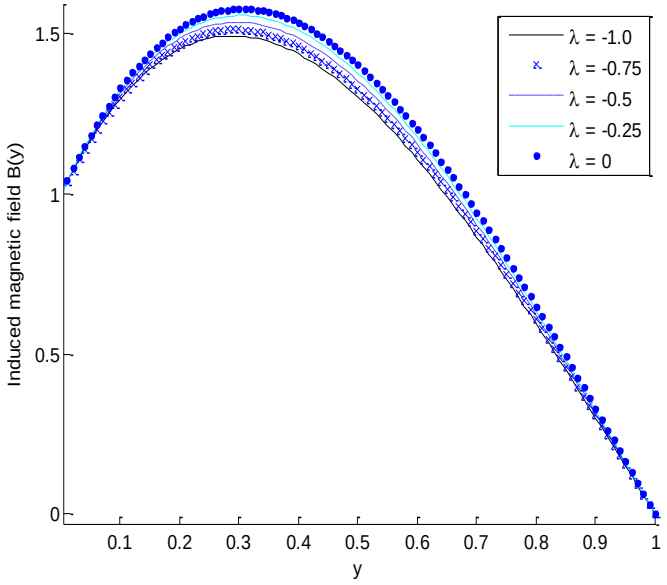

Figure 7. Effect of λ on induced magnetic field for different values of $(Ha = 4.0, Pm = 0.4,\ \varepsilon = 0.1)$.

diffusivity. This weakens the Lorentz force's damping effect, allowing the fluid velocity to rise. Consequently, lower values of the magnetic Prandtl number lead to higher velocity profiles, whereas higher values result in reduced velocities because of stronger magnetic damping. Understanding this behaviour is crucial for several practical applications. It aids in optimising liquid metal flow in MHD generators, controlling heat and mass transfer in nuclear reactors, and improving metallurgical processes

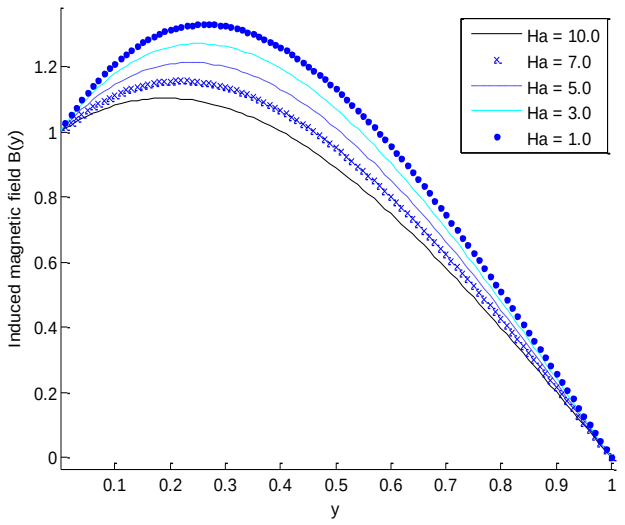

Figure 8. Effect Ha on induced magnetic field for different values of $(Pm = 0.4, \varepsilon = 0.1,\ \lambda = -1.0)$

such as steel and aluminium casting. It is also important for managing cooling in high-performance electronic devices operating in magnetic environments. Additionally, this insight is relevant to biomedical applications involving magnetic field-assisted therapies, where precise control of fluid motion is essential.

As viscosity increases, the fluid motion becomes more restrained, resulting in prolonged interaction with the magnetic field. This enhances shear effects and amplifies the influence of the induced Lorentz force. Consequently, these combined factors contribute to an increase in the induced magnetic field, as demonstrated in Figure 7. This phenomenon has practical significance in several engineering and industrial contexts, including the design and optimisation of MHD generators, control of liquid metal flows in metallurgical processes, enhancement of cooling efficiency in nuclear reactors, and regulation of conductive fluid flow in high-performance electronic devices. It is also relevant in biomedical applications such as magnetic field-assisted drug delivery or targeted fluid manipulation, where controlling the induced magnetic field is critical for precision and safety.

Figure 8 depicts the variation of the induced magnetic field strength across the channel for different Hartmann numbers. As the Hartmann number increases, the induced magnetic field is significantly suppressed. This effect is primarily due to the Lorentz force, which acts as a damping mechanism in magnetohydrodynamic (MHD) flows. At lower Hartmann numbers, the magnetic field exerts a weaker influence, allowing the conductive fluid to flow more freely. Consequently, stronger velocity gradients are established, which enhance magnetic field induction through the increased motion of charged particles in the fluid. Understanding this behaviour is crucial for practical applications such as the design and optimisation of MHD

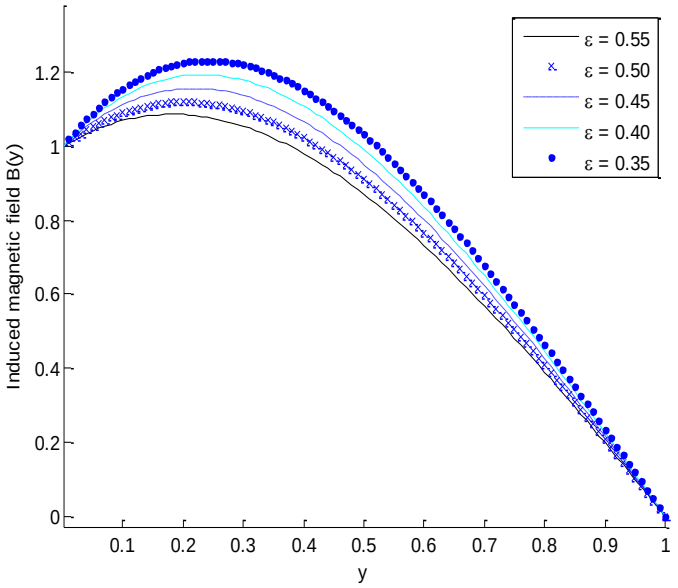

Figure 9. Effect of ε on induced magnetic field for different values of $(Ha = 4.0, Pm = 0.4, \quad \lambda = -1.0)$

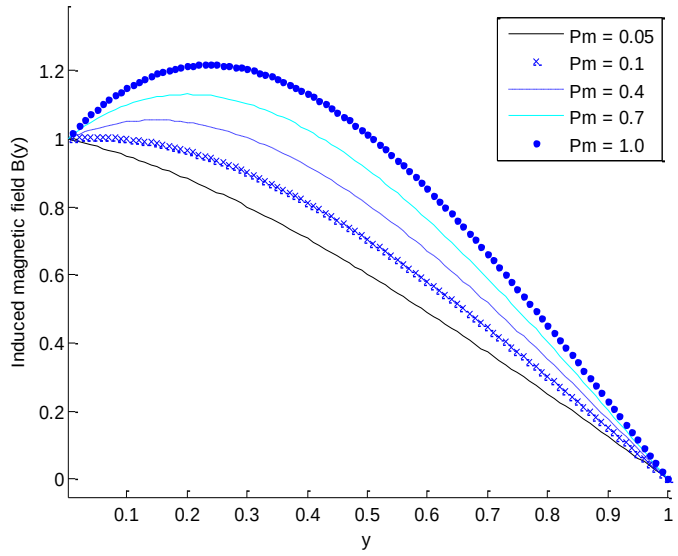

Figure 10. Effect of Pm on induced magnetic field for different values of $(Ha = 4.0, \quad \varepsilon = 0.1, \lambda = -1.0)$

generators, control of molten metal flows in metallurgical processes, regulation of cooling in nuclear reactors, and management of conductive fluid flow in high-performance electronic devices. It is also relevant in biomedical applications, where magnetic field manipulation is used for targeted therapies or precision control of conductive fluids.

Figure 9 illustrates the effect of thermal conductivity on the induced magnetic field. The results indicate that lower values of thermal conductivity enable the conductive fluid to maintain higher velocity gradients, thereby enhancing the generation of induced magnetic fields. In contrast, higher thermal conductivity values are associated with increased resistance, either thermal or viscous, that suppresses fluid motion and diminishes the induced magnetic field strength. This behaviour underscores the interaction between fluid transport properties and electromagnetic effects in magnetohydrodynamics (MHD) flows. The enhanced induced field observed at lower thermal conductivity reflects the fluid's greater ability to dynamically respond to the applied magnetic field.

Figure 10 illustrates the effect of the magnetic Prandtl number on the induced magnetic field. The results show that the strength of the induced field increases with higher magnetic Prandtl numbers. This behaviour is due to the reduced magnetic diffusivity at elevated magnetic Prandtl numbers, which allows the magnetic field lines to remain more closely aligned with the motion of the conducting fluid. As a result, the fluid flow more effectively amplifies the induced magnetic field, enhancing electromagnetic interactions within the system. This phenomenon has practical significance in a variety of applications. It is important for improving the efficiency of MHD generators and optimising liquid metal cooling in nuclear reactors. Moreover, it plays a key role in electromagnetic flow control in metallurgical processes, such as aluminium and steel casting, and in advanced biomedical devices that utilise magnetic field-assisted fluid manipulation, including targeted drug delivery systems.

Table 1 illustrates the effects of viscosity and thermal conductivity on the skin friction at both plates. It is observed that a decrease in viscosity results in increased skin friction on the moving plate, while the opposite trend occurs on the stationary plate due to reduced momentum diffusion. Furthermore, the table indicates that variable thermal conductivity tends to decrease skin friction on the moving plate but increases it on the stationary plate, reflecting the influence of enhanced heat transfer and its impact on flow gradients near the surfaces.

Table 2 shows the computed effects of the Hartmann number and magnetic Prandtl number on skin friction on both plates. The results indicate that an increase in these parameters leads to higher skin friction on the moving plate, while the reverse trend is observed on the stationary plate. This behaviour is physically attributed to the intensified Lorentz force arising from stronger magnetic effects, which enhances the velocity gradient near the moving plate and concurrently reduces momentum transfer to the stationary plate

Table 3 highlights the influence of thermal conductivity on the rate of heat transfer on both plates. The findings reveal that increasing thermal conductivity enhances heat transfer on the moving plate, while the opposite effect occurs on the stationary plate. Physically, this is because higher thermal conductivity amplifies temperature gradients near the moving plate, thereby increasing heat

Table 1. The effect of viscosity and thermal conductivity on skin friction at the plate $y = 0$ and $y = 1$.

λ	$(Pm = 0.4, Ha = 4.0, \varepsilon = 0.1)$		ε	$(Pm = 0.4, Ha = 4.0, \lambda = -1.0)$	
	τ_0	τ_1		τ_0	τ_1
-0.25	3.5660	0.2400	0.15	5.2784	0.1021
-0.5	4.0155	0.1789	0.35	5.1823	0.1498
-0.75	4.5817	0.1273	0.55	5.0744	0.2037
-1.0	5.3004	0.0912	0.85	4.8952	0.2938

Table 2. The effect of Hartmann number and magnetic Prandtl number on skin friction at the plate $y = 0$ and $y = 1$.

Ha	$(\varepsilon = 0.1, Pm = 0.4, \lambda = -1.0)$		Pm	$(\varepsilon = 0.1, Ha = 4.0, \lambda = -1.0)$	
	τ_0	τ_1		τ_0	τ_1
2.0	2.9709	0.8009	0.1	4.7056	0.6859
2.5	3.5161	0.5407	0.4	5.3004	0.0912
3.0	4.0861	0.3053	0.7	5.8951	0.0453
3.5	4.6808	0.0947	1.0	6.4899	0.0193

Table 3. The effect of thermal conductivity on rate of heat transfer at the plate $y = 0$ and $y = 1$.

ε	$(Pm = 0.4, Ha = 4.0, \varepsilon = 0.1)$	
	τ_0	τ_1
0.15	1.0087	0.8505
0.35	1.0504	0.6490
0.55	1.1330	0.4369
0.85	1.3602	0.0687

flux, whereas it tends to diminish temperature gradients near the stationary plate, leading to a reduction in heat transfer.

Finally, results obtained from this study indicate a combination of agreement and meaningful improvements over those of previous studies, especially that of Ajibade and Bolaji (2020), whose mathematical model was adopted in the present study. Whereas Ajibade and Bolaji solved the coupled nonlinear differential equations using the Differential Transform Method, the study at hand applied the Homotopy Perturbation Method (HPM) under the same boundary conditions. The HPM approach produced convergence that is faster, more computationally efficient, and better reflects the underpinning physics of Couette flow. Furthermore, the prevailing literature has often failed to include the synergistic impact of temperature-dependent viscosity, temperature-dependent thermal conductivity, and the induced magnetic field. The study at hand has bridged this knowledge gap in providing additional insights on how variable fluid properties interact with MHD flow, a very important flow regime that has functional application in practical engineering and industrial processes. In addition, this present study supports the prevailing observation that the exclusion of temperature-dependent viscosity and thermal conductivity inevitably results in misleading or spurious predictions from natural convection problems. The present results reinforce the need to properly model these variable properties to obtain reliable thermodynamic and flow-field characteristics.

More specifically, the findings of the present study are in line with previous research (Ajibade and Bolaji, 2020) by establishing that:

1. The velocity profile decreases with an increase in fluid viscosity, magnetic Prandtl number, Hartmann number, and a decrease in thermal conductivity.
2. This observation agrees with the classical theory of MHD flow that expects higher magnetic and viscous forces to act against the motion of the fluid.
3. Temperature profiles decrease as the value of the thermal conductivity parameter increases, which validates that increased heat conduction reduces the temperature of the fluid by facilitating faster thermal diffusion.
4. The profile of the induced magnetic field increases when the magnetic Prandtl number is raised and the fluid viscosity is lowered.

This behaviour is consistent with theoretical expectations, since smaller viscosity is conducive to stronger coupling between fluid motion and magnetic induction. Overall, the present findings support many aspects of earlier studies (Ajibade and Bolaji, 2020). However, they uniquely extend the literature by demonstrating how variable viscosity, variable thermal conductivity, and induced magnetic fields collectively influence MHD Couette flow. This integrated perspective provides a more accurate and practically relevant understanding than is typically found in prior work.

CONFLICT OF INTEREST

The authors declare that they have no conflict of interest.

REFERENCES

Abdul-Ameer, A. Y., & Abdul-Sattar J. A. A. (2023). Fourier-homotopy perturbation method for heat and mass transfer with 2D unsteady squeezing viscous flow problem. *Journal of Computational Applied Mechanics, 54*(2), 219-235.

Adnan, K. F., & Osama. H. M. (2023). Homotopy perturbation method for solving time-fractional nonlinear variable-order delay partial differential equations. *Partial Differential Equations in Applied Mathematics, 7*, 100513.

Ajibade, A. O., & Bolaji, A. S. (2020). Steady natural convection MHD flow in a vertical channel with induced magnetic field and variable fluid properties. *The Journal of the Mathematical Association of Nigeria, 47*(1), 176- 192.

Ajibade, A. O., & Ojeagbase, P. O. (2019). Effects of variable viscosity and thermal conductivity on free convection heat and mass transfer flow through a vertical channel. *J Appl Computat Math*, *8*(441), 2-7.

Ajibade, A. O., & Tafida, M. K. (2020). The combined effect of variable viscosity and variable thermal conductivity on natural convection couette flow. *International Journal of Thermofluids*, *5*, 100036.

Ajibade, A. O., & Umar, A. M. (2020). Mixed convection flow in a vertical channel in the presence of wall conduction, variable thermal conductivity and viscosity. *Nonlinear Engineering*, *9*(1), 412-431.

Bichi, Y. A., & Ajibade, A. O. (2020). Combined effects of variable viscosity, viscous dissipation and thermal radiation on unsteady natural convection couette flow through a vertical porous channel. *FUDMA Journal of Sciences, 4*(2), 135-150.

Borgohain, D. (2023). Impacts of temperature dependent thermal conductivity and viscosity on slipped flow of Maxwell nanofluid. *East European Journal of Physics, 4*, 120-128.

Das, U. J., & Patgiri, I. (2024a). Influences of variable viscosity and variable thermal conductivity on a mixed convective hydromagnetic flow in a vertical channel with thermophoretic deposition. *Journal of Engineering Physics and Thermophysics, 97*, 733-744.

Das, U. J., & Patgiri, I. (2024b). Entropy analysis on Thermophoretic magnetohydrodynamic couette flow over a deformable porous channel with temperature-dependent viscosity and thermal conductivity, 53(5), 2556-2571.

Erinle-Ibrahim, L. M., Babajide, Idowu, A. O., & Oluwatobi, I. K. (2021). Application of Homotopy perturbation method to the mathematical Modelling of temperature rise during microwave hyperthermia. *FUDMA Journal of Sciences, 5*(2), 273-282.

Farhood, A. K., & Mohammed, O. H. (2023). Homotopy Perturbation Method for solving time-fractional nonlinear variable-order delay partial differential equations. *Partial Differential Equations in Applied Mathematics, 7*, 100513.

Gouder, P.M., Kolli, V.H., Hanif, M. D., Krishna B. C., & Praveen, C. (2022). The homotopy perturbation method to solve a wave equation. *Communications in Mathematics and Applications, 13*(2), 691-701.

Hamza, M. M., Ejiwole, O. J., Usman, H., Almu, A., Hamisu, A., & Musa, M. (2024b). Effect of variable thermal conductivity on oscillatory magnetized couette flow in a channel filled with porous material. *UMYU Scientifica, 3*(4), 218-231.

Hamza, M. M., Suleiman, B. A. Ahmad, S K., & Ahmad, R. T. (2024a). Nonlinear-mixed convection flow with variable thermal conductivity impacted by asymmetric/symmetric heating/cooling conditions. *Arabian Journal for Science and Engineering, 49,* 14763-14772.

Hazarika, G. C., & Konch, J. (2016). Effect of variable viscosity and thermal conductivity on magnetohydrodynamic free convection dusty fluid along a vertical porous plate with heat generation. *Turkish Journal of Physics, 40*, 52-68.

Jha, B. K., & Aina, B. (2017). Impact of induced magnetic field on MHD mixed convection flow in vertical microchannel formed by non-conducting and conducting infinite vertical parallel plates. *Journal of Nanofluids, 6*, 960-970.

Jha, B. K., & Malgwi, P. B. (2022). Hydromagnetic free convection flow in a vertical microporous channel with Hall current and ion-slip effect. *Journal of the Egyptian Mathematical Society*, *30*(1), 21.

Jyothi, K., Venkateswarlu, B., Reddy, P. C., Kodi, R., & Annapureddy, D. R. (2025). Neural network-driven analysis of MHD boundary layer flow and heat transfer in Sisko nanofluids. *Multiscale and Multidisciplinary Modelling, Experiments and Design*, *8*(6), 291.

Kaita, I. H., Zayyanu, S. Y., Mas'ud, L., Hamsiu, A., Abdullahi, U., & Auwal, D. M. (2024). Heat and mass transfer flow in a channel filled with porous medium in the presence of variable thermal conductivity. F*UDMA Journal of Sciences*, 8(2), 225-234.

Kalyan, S., Kandagal, M., Tawade, J. V., Satpute, N., Khan, M. I., Kulkarni, N., ... & Gupta, M. (2025). Exploring Mixed Convection in Porous Media: Thermal and Flow Behaviour. *Partial Differential Equations in Applied Mathematics*, *15,* 101239.

Kandagal, M., & Kempepatil, R. (2024). An investigation of the heat and mass transfer effects in vertical channels with immersible fluid flow through a porous matrix. *ZAMM‐Journal of Applied Mathematics and Mechanics/Zeitschrift für Angewandte Mathematik und Mechanik*, *104*(10), e202300998.

Kandagal, M., Kempepatil, R., Tawade, J. V., Nazarova, N., Gupta, M., & Khan, M. (2025). The impact of carbon nanotubes (CNT) on heat generation and absorption, the behaviour of water and blood suspensions in an inclined channel with a porous matrix. *Partial Differential Equations in Applied Mathematics*, *15*, 101241.

Khaleghizadeh, S. (2022). Homotopy perturbation method with the help of Adomian decomposition method for nonlinear problems. *Mathematical Analysis and its Contemporary Applications, 4*(1); 45-51.

Konduru, V. R., Narahari, R. B., Poli, C. R., Battala, V. S., Ravuri, M. R., Dandu, S., & Balaraju, M. R. A. MHD flow and heat transfer of carreau fluid with radiation and heat source effect.

Journal of Advanced Research in Numerical Heat Transfer, 26(1), 141-155.

Kumar, K. T., Kalyan, S., Kandagal, M., Tawade, J. V., Khan, U., Eldin, S. M., ... & Abed, A. M. (2023). Influence of heat generation/absorption on mixed convection flow field with porous matrix in a vertical channel. Case Studies in Thermal Engineering, *47*, 103049.

Meruva, P., Reddy, P. C., Roja, P., & Leela, R. A. (2022). Characteristics of MHD three-dimensional flow of nanofluid over a permeable stretching sheet. *Heat Transfer, 51*, 3586-3599.

Mottupalle, G. R., Ashwathnarayana, D. P., Shankarappa, B. M., & Sanjeevamurthy, A. A. (2022). Effects of variable fluid properties on double diffusive mixed convection with chemical reaction over an accelerating surface. *Biointerface Research in Applied Chemistry, 12*(4), 5161-5173.

Omokhuale, E., & Ojemeri, G. (2024). Couette Flow in the presence of viscous dissipative fluid along an upstanding channel affected by newtonian heating: Homotopy perturbation approach. *Journal of Basic Physical Research, 12*(1), 1 – 12.

Reddy, P. C., Umamheswar, M., Reddy, S. H., Raju, A. M., & Raju, M. C. (2022). Numerical study on the parabolic flow of MHD fluid past a vertical plate in a porous medium. *Heat Transfer*, *51*(4), 3418-3430.

Saini, G., Hanumagowda, B. N., Varma, S. V. K., Chohan, J. S., Shah, N. A., & Jeon, Y. (2023). Impact of couple stress and variable viscosity on heat transfer and flow between two parallel plates in conducting field. *AIMS Mathematics, 8*(7), 16773-16789.

Saravanakumar, S., Eswari, A., Makinde, O. D., Anbazhagan, N., Joshi, G. P., & Cho, W. (2023). Analysis of temperature-dependent thermal conductivity and fin efficiency: Direct Akbari-Ganji method. *Case Studies in Thermal Engineering, 51*, 103627.

Sharahy, A., & Sawlan, Z. (2023). Estimation of Temperature-Dependent Thermal Conductivity and Heat Capacity Given Boundary Data. *Computation*, *11*(9), 184.

Singh, V., & Argawal, S. (2013). Flow and heat transfer of maxwell fluid with variable viscosity and thermal conductivity over an exponentially stretching sheet. American Journal of Fluid Dynamics, 3(4), 87-95.

Sobamowo, M. G. (2023). Direct applications of homotopy perturbation method for solving nonlinear algebraic and transcendental equations. *International Journal of Petrochemical Science and Engineering, 6*(1), 10-22.

Tafida, M. K. Abdullahi, A. Y., & Auwal, N. (2025). Magnetohydrodynamics Effects on Steady Natural Convection Couette Flow of Heat Generating/Absorbing Fluid in a Vertical Channel with Viscous Dissipation. *FUDMA Journal of Sciences, 9*(6), 375-383.

Tafida, M. K., & Ajibade, A. O. (2019). Effect of variable viscosity on natural convection flow between vertical parallel plates in the presence of heat generation/absorption. *Asian Research Journal of Mathematics, 14*(3), 10-15.

Tafida, M. K., & Tajuddeen, A. (2024). Homotopy perturbation method for analysing the effect of viscous dissipation on steady natural convection Couette flow with convective boundary conditions. International Journal of Fluid Mechanics and Thermal Sciences, 10(3), 45-56.

Tafida, M. K., Ajibade, A. O., & Lawal, U. (2021). Effects of Variable Viscosity and Thermal Conductivity on Steady Natural Convection Couette Flow Having Suction/Injection. T*ransactions of the Nigerian Association of Mathematical Physics,* 15(April –June, Issue), 139-150.

Tafida, M. K., Ajibade, A. O., & Usman, M. H. (2020). Effects of variable viscosity and viscous dissipation on free convective couette flow in a vertical channel: The homotopy perturbation method approach. *Abacus (Mathematics Science Series)*, *47*(1), 161 -175.

Umamaheswar, M., Reddy, P. C., Reddy, S. H., Mopuri, O., & Ganteda, C. K. (2022). Aspects of parabolic motion of MHD fluid flow past a vertical porous plate with cross-diffusion effects. *Heat Transfer*, *51*(5), 4451-4465.